III. RESPONSE AND FAILURE OBSERVATION OF WEAKLY DESIGNED STEEL STRUCTURE MODELS

(Part 2) Elastic and Inelastic Responses Observed on October 4 in 1985

by

Koichi TAKANASHI (I) and Kenichi OHI (II)

1. INTRODUCTION

It is well recognized that complicated vibrations are induced during earthquakes in structures, their basements, and their surrounding soils, and these behaviors greatly influence structural failures. In earthquake resistant design, it is a very important problem to predict the responses of these soil-structure systems including their inelastic behaviors. To obtain this solution, it is also indispensable to collect their actual responses to natural earthquakes.

From this point of view, an observation project of weakly designed steel structure models began in the Chiba Experiment Station of Institute of Industrial Science, University of Tokyo, since August in 1983 [1]. During two years, many small earthquakes were recorded, but their intensities were too small to damage the structure models. At night on October 4 in 1985, a strong earthquake occurred, the acceleration of which reached to about 80 gals in the observation site. One of the steel structure models was inelastically damaged by this earthquake for the first time in this project. This paper describes an outline of their responses to October 4 earthquake.

2. STRUCTURE MODELS AND INSTRUMENTATION

Two models were constructed on the actual ground. The outline of each model is summarized as follows:

(1) Model No.1

A three-story moment resistant frame composed of H-shaped columns (H-125x125x6.5x9) and H-shaped girders; x and y directions shown in Fig. 1 coincide with the weak-axis and the strong axis of H-shaped column section, respectively.

(2) Model No.2

A three-story braced frame composed of H-shaped columns (H-150x50x5x7), H-shaped girders, and braces; the braces of x-direction (weak-axis of column section) are composed of rectangular section parts (plate 6x10x400) and angle parts (L-75x75x6), and the braces of y-direction are composed of angle members (L-75x75x6). The y-direction braces are installed for preventing catastrophic collapse due to rotational movements after irregular

(I) Professor, (II) Research Associate of Institute of Industrial Science, University of Tokyo

buckling of x-direction braces, and they are scheduled to be removed in the near future. The yield base shear force of x-direction is 9 % of total building weights, and this strength is less than one-third of the design practice in Japan.

The reinforced concrete basements (5 meters square) were installed directly on the surface of Kanto loam after top soil was removed. The profiles of the soils are shown in Fig. 2[2]. The shapes and the dimensions of the two models are shown in Figs. 3 and 4, and the fundamental parameters are summarized on Tables 1 and 2.

Various types of transducers were installed on the models to measure the following data:

1) Accelerations of each floor, 3x3 components per model.
2) Accelerations of basement, 3 components per model.
3) Inter-story displacements including rotation, 4x3 components per model.
4) Flexural strains of 1st story column and Axial strains of braces, 32 components per model.

Additionally the underground accelerations at the depths of 1 meter, 10 meters, 20 meters, and 40 meters are recorded simultaneously. The data acquisition is automatically started once 1 gal is sensed at the depth of 40 meters, and the data are converted into digital form with the sample time of 5 milliseconds.

3. SUMMARY OF RESPONSE OBSERVATION

The earthquake described herein occurred at 9:26 p.m. on October 4 in 1985, and its unusual strong ground motion astonished many citizens in the metropolitan area. According to the announcement of Japan Meteorological Agency, the magnitude of this earthquake is 6.2 and the epicenter is located at Lat.35^{o}53' N. and Long.140^{o} 9' E. on the boundary of Chiba and Ibaragi Prefectures, 30 kilometers distant from the observation site.

Fig. 5 shows the time histories of acceleration records in each directions, x and y, of the two steel models. The underground accelerations recorded at 5 meters close to the model No.2 are modified into the records along the x and y directions and also shown in Fig. 1. It is found that the considerable magnification of acceleration is induced in the upper parts of soil less than 10 meters deep.

The peak values of observed responses, such as accelerations, story shears, and drifts are summarized in Table 3. Story shear coefficients (story shears normalized by the sum of the upper floor weights) are also shown with parentheses in Table 3. The 1st story shears in all the models reach to more than 8 % of total building weights. High acceleration and story shears are observed in the y-direction of the model No.2. This is explained by the coincidence of the natural frequency of this direction with the dominant one of the excitation wave. There are no damages in this direction, however, because the model is sufficiently strengthened by the angle braces in this direction. On the other hand, the weakly designed braces in the x-direction of the model No.2 experienced buckling and considerable yielding. The peak drift of the 1st story is 0.46 centimeters, and the

permanent deformation of 0.2 centimeters remain after the earthquake. The responses of the model No.1, designed stronger than the model No.2, remain in elastic ranges.

4. INELASTIC BEHAVIOR OF BRACED FRAME

In the x-direction of the model No.2 the 1st story braces experienced buckling and considerable yielding. The base shear vs. drift curve and their time histories are shown in Figs. 6 and 7. After several reversals in elastic ranges, the buckling of the compression-side bars occurred and the maximum strength of the 1st story (point A shown in Figs. 6 and 7) was observed. In this moment the tension-side bars seemed to yield already. The softening of the initial stiffness due to various imperfections in the compression-side bars allows the tension-side bars to yield before the buckling of the compression-side ones. This presumption is supported by the following fact; the calculated initial stiffness (broken line in Fig. 6), by assuming that the both-side bars are completely effective, considerably overestimates the observed initial stiffness. In the evaluation of the initial stiffness k the following formula is used:

$$k = 2\,N\,E\,Aeq\,(\text{cosine}\,\theta)^2 / l_b \qquad (1)$$

where E : Young's modulus, set to 2100 ton/cm .
l_b : total length of the brace
θ : the angle between the axis of bars and the horizontal line
N : number of pairs of bars
Aeq : equivalent sectional area of brace composed of two kinds of members, calculated by:

$$Aeq = l_b / \left(\frac{l_1}{A_1} + \frac{l_2}{A_2}\right) \qquad (2)$$

where l_1, l_2 : length of two different members
A_1, A_2 : sectional area of two different members. Subscript 1 and 2 correspond to the plate 6x10x400 and the angle members L-65x65x6, respectively. As for A_2, the half area of one flange is ignored.

The unloading stiffness after yielding can be evaluated by the half of eq.(1), also shown as broken line in Fig. 6. Other components of stiffness, such as column stiffness and the decrement of stiffness due to so-called P- Δ effects, are so much smaller than the brace stiffness as to be ignored in the evaluation.

The maximum load-carrying capacity Pmax (point A in Fig. 6) can be evaluated by the sum of the buckling load in compression-side bars and the yield load in tension-side bars:

$$Pmax = N (\sigma_y A_1 + \sigma_{cr} A_1) \cdot \text{cosine } \theta \quad (3)$$

where σ_{cr} : Euler's buckling stress
σ_y : yield stress

As for the evaluation of the buckling stress, it is assumed by considering the bar-end conditions that the effective buckling length is 60 % of the clear length. Calculated Euler's buckling stress is about 1.0 ton/cm^2. As for the evaluation of the yield stress, the strain-rate effects on yields stress should be considered. Fig. 8 shows the results of tension tests on brace materials. As is often experienced, under the higher strain rate the yield stress slightly increases. The duration of yielding from the point A to the unloading point B shown in Fig. 6 is very short time of 0.1 seconds, and the averaged strain rate comes up to 0.12 per second. Although this is out of the above test ranges, the extrapolated value 3.5 ton/cm^2 is used for the yield stress. The evaluated load-carrying capacity is also plotted in Fig. 6.

5. SPECTRAL ANALYSES AND NATURAL FREQUENCIES

Since the efficient algorithm of the fast Fourier transform was presented by Cooley and Tukey in 1965, the finite Fourier components of discrete time series can be rapidly and easily computed by many researchers and engineers. Also in this report the FFT techniques are utilized in order to identify the spectral characteristics of the soil-structure interaction systems. The data processing in the system identification was carried out in the following way[3]:

(1) Consider the unknown system, whose input and output time series are denoted by $x(t)$ and $y(t)$, respectively, as shown in Fig. 9. The Fourier transforms of these time series, $X(\omega)$ and $Y(\omega)$, can be approximated by the finite complex Fourier components in the FFT computation. The data length used is 40.96 seconds and the data size is 8192.

(2) The energy spectrum or the Fourier square amplitude spectrum of the input time series, denoted by Sxx, and the cross spectrum of the input and output time series, denoted by Sxy, are calculated under the following definitions:

$$Sxx = X^*(\omega) \cdot X(\omega) \quad (4)$$

$$Sxy = X^*(\omega) \cdot Y(\omega) \quad (5)$$

where $X^*(\omega)$ denotes the conjugate of $X(\omega)$.

Evidently Sxx and Sxy indicate the contribution of each spectral component to the two integrals $\int_{-\infty}^{\infty}(x(t))^2 dt$ and $\int_{-\infty}^{\infty} x(t)y(t)\, dt$, respectively.

(3) The FFT techniques have high resolving capacity, but the computed spectral values often shows abrupt changes, which may be caused by some errors included in the data. In order to remove these unstable changes and to pay attention to slowly changed

essentials, some smoothing techniques are applied to the spectral values. In this report, the computed spectral values, Sxx and Sxy, are smoothed by a rectangular spectral window, the band width of which is set to 0.3 Hz. This smoothing process makes no change in the original values of the two integrals $\int_{-\infty}^{\infty}(x(t))^2 dt$ and $\int_{-\infty}^{\infty}x(t)y(t)dt$. Smoothed energy spectrum and smoothed cross spectrum are denoted by $\overline{Sxx}$ and $\overline{Sxy}$, respectively.

(4) The system function of this input-output system, denoted by $H(\omega)$, is defined as a complex function, which satisfies the following equation:

$$Y(\omega) = H(\omega) \cdot X(\omega) \tag{6}$$

The system function $H(\omega)$ can be identified by:

$$H(\omega) = \overline{Sxy} \,/\, \overline{Sxx} \tag{7}$$

In this report four kinds of observed acceleration records, which are recorded at 1) -40m underground, 2) -1m underground, 3) basement, 4) roof floor, are chosen to identify three kinds of input-output system, from 1) to 2), from 2) to 3), and from 3) to 4). Smoothed Fourier amplitude spectra of the above four kinds of records and the three system gains are shown in Figs. 10 to 13 for each directions of the two models. In Figs. 10 to 13, square root values of the smoothed energy spectra are plotted as the smoothed Fourier amplitude spectra, and absolute values of system functions identified by eq.(7) are plotted as the system gains.

In the system gains from -40 m to -1 m underground accelerations, three peaks at 2 Hz, 5.5 Hz, and 8.5 Hz are commonly observed in four cases. As for the system gains from -1 m underground to the basement, the gains for the frequencies less than 5 Hz can be regarded as almost unit except in the y-direction of the model No.2. In other words, except in the y-direction of the model No.2, the basements and the soil of 1 meter depth show almost the same motions at least for the components of frequencies less than 5 Hz. The gains decrease for the frequencies greater than 5 Hz, and the systems behave as so-called low-pass filters. One of possible explanations for this phenomenon is the following one: when the motion of soil surface consists of different phase components and the basement restrain them, the high-cycle components, the wave length of which is shorter than the size of the basement, will be cut off in the motion of the basement[4]. In the y-direction of the model 2, the gain of 4.5 Hz is dominant, and this frequency agrees with the dominant frequency of the upper model. This fact shows the existence of the interacted motion between the basement and the upper structure, such as rocking movements.

The system gains from the basement to the roof response are characterized with natural frequencies peculiar to each models. Eigen value analyses on simple vibrational models shown in Fig. 14 were made to explain the natural frequencies observed in the system gains. The values of the story stiffness used in model A, B, C, and E (Fig.14) are the elastic ones derived from the observed story shear vs. story drift curves in each directions of the two models. In the model D, the 1st story stiffness in the

model C is substituted by the softened stiffness after yielding (see Fig. 6). In these models, the supporting conditions are assumed to be fixed. In the model F, the upper structure is assumed to be rigid, and the rocking of the basement is considered. As for the rocking stiffness denoted by K, the following approximate solution[5] for the semi-infinite elastic soil under the assumption of the triangular stress distribution shown in Fig. 15 is used:

$$K = \frac{1.513\pi b^3 \rho Vs^2}{2(1-\nu)} \tag{8}$$

where ρ : density of soil
b : length of basement side
Vs : shear wave velocity
ν : Poisson's ratio of soil

Calculated natural frequencies based on these vibrational models are summarized in Table 4. These calculated frequencies are also marked in Figs. 10 to 13. It is found that the above vibrational models well explain the identified natural frequencies.

6. COMPARISON WITH PAST ON-LINE SIMULATIONS

To study inelastic response behaviors of the model No.2, pseudo-dynamic tests were carried out on similarly fabricated model using the computer-actuator on-line system[1]. The details of the testing system have been already reported in Ref.[6]. In this system a loading test is carried out to measure the restoring force used in the numerical integration of equation of motion. Side view of the test setup is shown in Fig. 16, and the parameters used in the simulation are summarized on Table 5.

The wave shape of excitation used in the simulation is the NS component recorded at El Centro in 1940. Two phases of simulation were carried out with two input excitation levels; the peak values of acceleration were set to 130 gals and 160 gals. Simulated hysteresis loops of the 1st story are shown in Fig. 18(a) and (b). The hysteresis loop to October 4 earthquake is also shown again in Fig. 18(c).

The differences in the damage degrees shown in Fig. 18 correspond to the differences in the load effects of the three earthquakes. Response spectra of shear coefficient (1 % of critical damping) to these earthquakes are shown in Fig. 17. Two kinds of natural fundamental periods, the initial period and the period after yielding, are also marked in Fig. 17. Between these periods the values of response spectra to October 4 earthquake are much smaller than those to El Centro excitations, and then, the observed damage is also small compared with the on-line simulations. It is found that the seismic input due to October 4 earthquake slightly exceeds the elastic limit of the model No.2.

7. CONCLUDING REMARKS

(1) An outline of the elastic and inelastic responses due to October 4 earthquake have been described. As a whole, the data acquisition system works well, and especially, inelastic responses of steel structure accompanied with buckling and yielding of the braces have been successfully recorded.
(2) System identification techniques using Fast Fourier Transform are applied to the observed acceleration records. Identified natural frequencies of the upper structural systems fairly agree with theoretical frequencies based on simple vibrational models. Identified system gains from the underground of 1 meter depth to the basement are found to behave as low-pass filters. These results can be used in the further study on the modelling of soil-structure interaction system.
(3) The model No.2 was slightly damaged beyond its elastic limits. Considering the spectral characteristics of the observed excitation, this damage is found to be predictable and to match with the results of past on-line simulations, which were carried out on the similarly fabricated model using El Centro NS excitations. The observed strain rates of the tension bars reached to 0.12 per second, and the effects of strain rates on yield stress should be considered if precise prediction of the load- carrying capacity is needed.

ACKNOWLEDGEMENTS

The authors would like to express their appreciation to Mr. Y. Shimawaki and Mr. H. Kondo, technical officials of Institute of Industrial Science, University of Tokyo, for their supports during this study.

REFERENCES

[1] Takanashi, K. and Ohi K.: "Response and Failure Observation of Weakly Designed Steel Structure Models (Part 1)," Bulletin of Earthquake Resistant Structure Research Center, No.18, March,1985
[2] Sato, N. and Katayama, T.: "Observation of Earthquake Ground Motions and Strains," SEISAN-KENKYU Vol.35, No.9, Sept. 1985. (in Japanese)
[3] Hino, M.: "Spectral Analysis," ASAKURA-SHOTEN Co., Inc. Oct. 1977 (in Japanese)
[4] Yamahara, H.: "Ground Motions during Earthquake and the In-Put Loss of Earthquake to Building Response (Part 1), (Part 2)," Transactions of the Architectural Institute of Japan, No.165, Nov. 1969, No.167, Jan. 1970 (in Japanese).
[5] Yamahara, H.: "Practical Solutions for Soil-Structure Interaction System," Shimizu Technical Report, No.1, Dec. 1971.
[6] Takanashi, K. and Ohi, K.: "Earthquake Response Analysis of Steel Structure by Rapid Computer-Actuator On-line System," Bulletin of Earthquake Resistant Structure Research Center, No.16, March 1983.

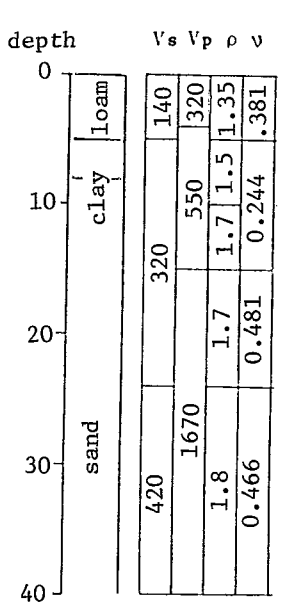

Vs : shear wave velocity (m/sec)

Vp : compression wave velocity (m/sec)

ρ : density (g/cm^3)

ν : Poisson's ratio

Fig. 2 PROFILES OF SOILS

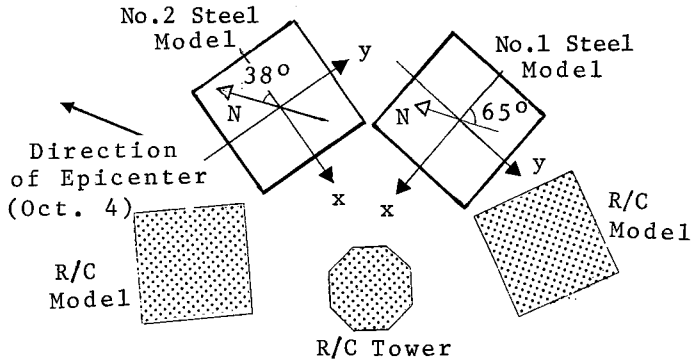

Fig. 1 LOCATIONS OF WEAKLY DESIGNED STEEL STRUCTURE MODELS

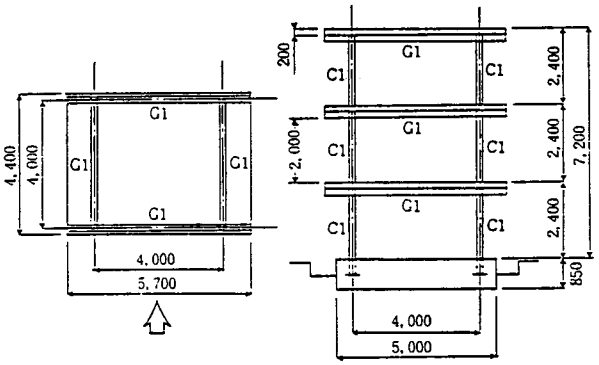

(1) Plan (2) Elevation

Fig. 3 SHAPES AND DIMENSIONS OF MODEL NO.1

Table 1 PARAMETERS OF MODEL NO.1

Stories	3
Area of Each Floor	25.1 m^2
Weight of Each Floor	12.7 tons
Steel Grade	JIS SS 41
Steel Members Used	C1 : H-125x125x6.5x9
	G1 : H-200x100x5.5x8
	Additional * L-65x65x6 Bracing

* Installed during maintenance work and storms

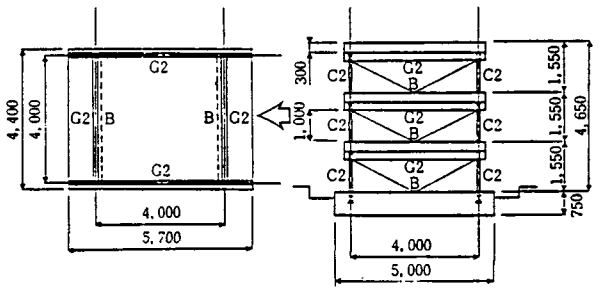

(1) Plan (2) Elevation

Fig. 4 SHAPES AND DIMENSIONS OF MODEL NO.2

Table 2 PARAMETERS OF MODEL NO.2

Stories	3
Area of Each Floor	25.1 m^2
Weight of Each Floor	17.6 tons
Steel Grade	JIS SS 41
Steel Members Used	C2 : H-100x50x5x7
	G2 : H-250x75x6x6
	B : PL-6x10
	Additional L-65x65x6 Bracing

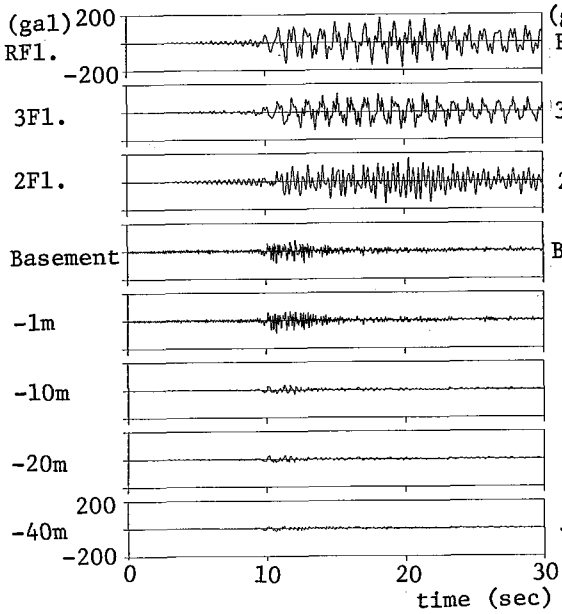

(1) No.1 —— x-direction

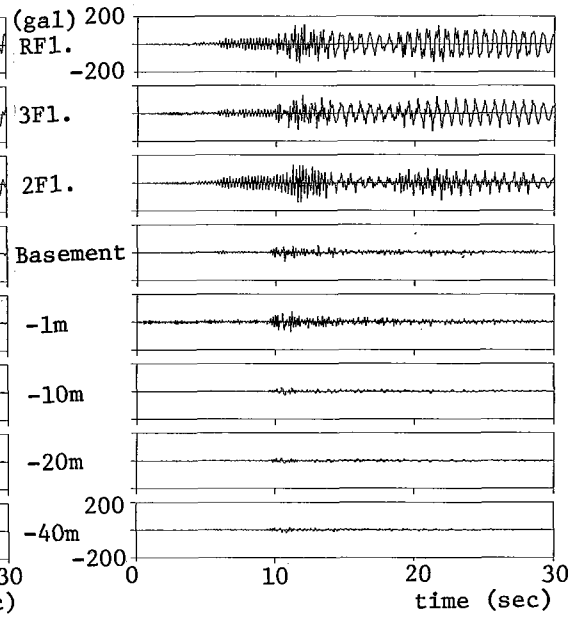

(2) No.1 —— y-direction

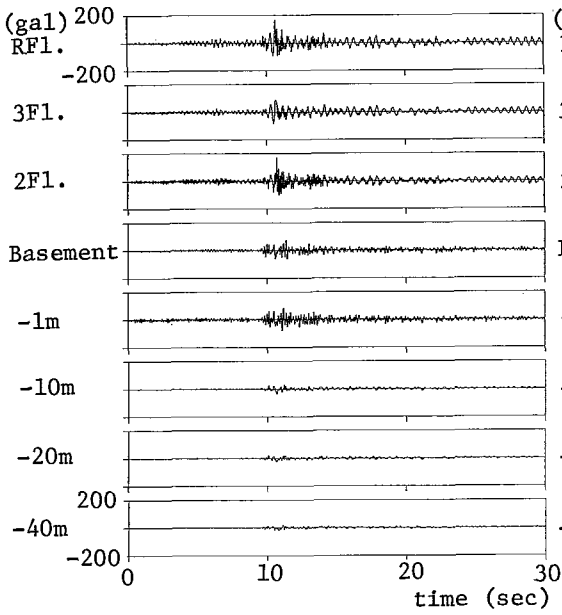

(3) No.2 —— x-direction

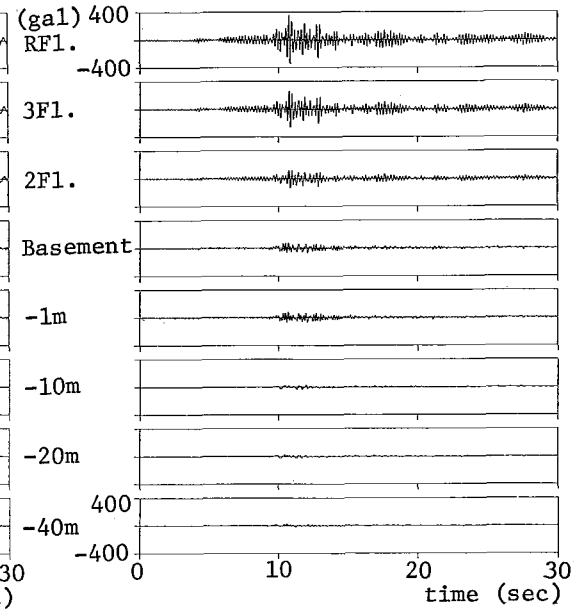

(4) No.2 —— y-direction

Fig. 5 TIME HISTORIES OF ACCELERATION OBSERVED

Table 3 PEAK VALUES OF RESPONSE OBSERVED

model		No. 1		No. 2	
direction		x (weak)	y (strong)	x (weak)	y (strong)
acc. (gal)	-40m	20	18	19	20
	-20m	29	21	25	26
	-10m	36	28	33	33
	-1m	88	77	84	86
	Basement	86	63	71	73
	2 Fl.	164	138	171	133
	3 Fl.	131	128	88	259
	R Fl.	180	139	165	352
story* shear (ton)	1st st.	3.0 (0.08)	3.5 (0.09)	4.8 (0.09)	13.1 (0.25)
	2nd st.	2.8 (0.11)	2.4 (0.09)	4.5 (0.13)	11.0 (0.31)
	3rd st.	2.3 (0.18)	1.8 (0.14)	3.0 (0.17)	6.3 (0.36)
story drift (cm)	1st st.	1.20	0.56	0.46	0.12
	2nd st.	1.11	0.40	0.11	0.08
	3rd st.	0.88	0.28	0.06	0.04

*Parenthesized values are story shear coefficients.

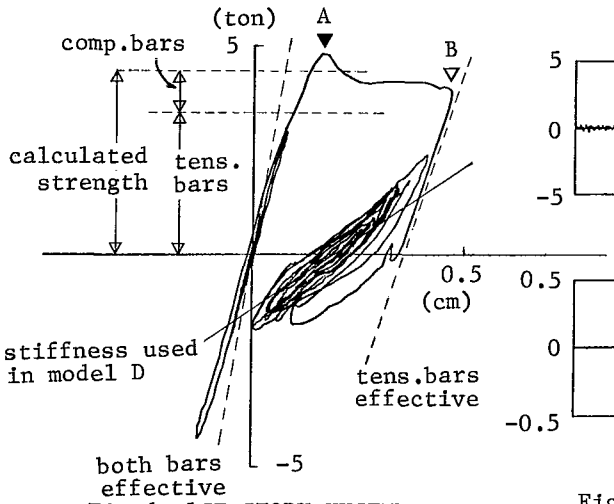

Fig.6 1ST STORY HYSTERESIS LOOP OF NO.1 MODEL IN X-DIRECTION

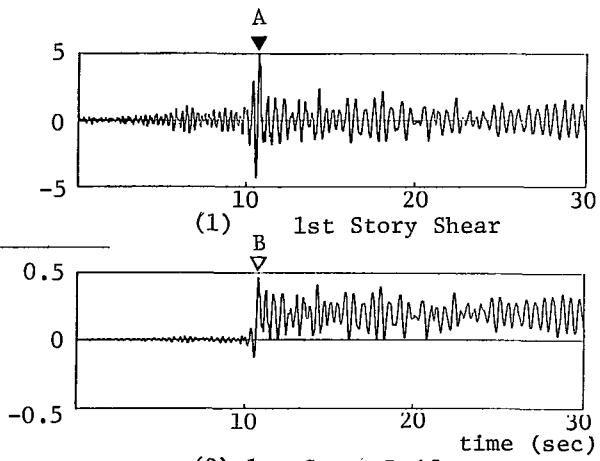

Fig. 7 TIME HISTORIES OF STORY SHEAR AND DRIFT

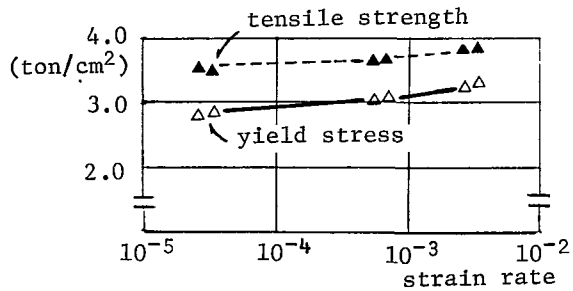

Fig. 8 TENSION TEST RESULTS OF BRACE MATERIAL

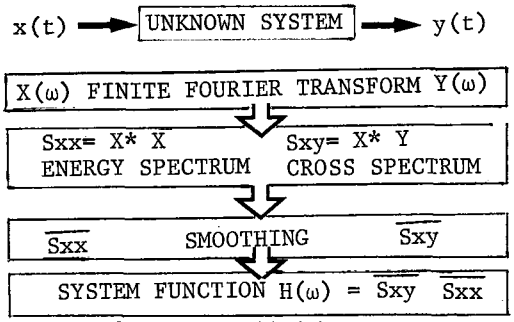

Fig. 9 FLOW DIAGRAM OF SYSTEM IDENTIFICATION

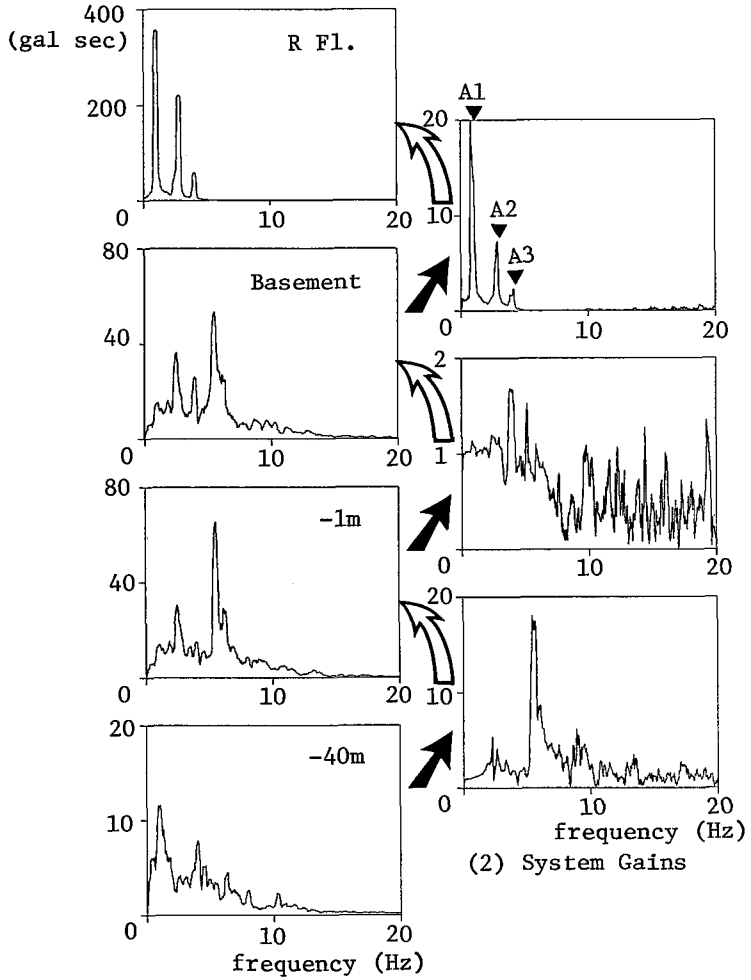

(1) Smoothed Fourier Amplitude Spectra

Fig. 10 FOURIER SPECTRA AND SYSTEM GAINS (MODEL NO.1, X-DIRECTION)

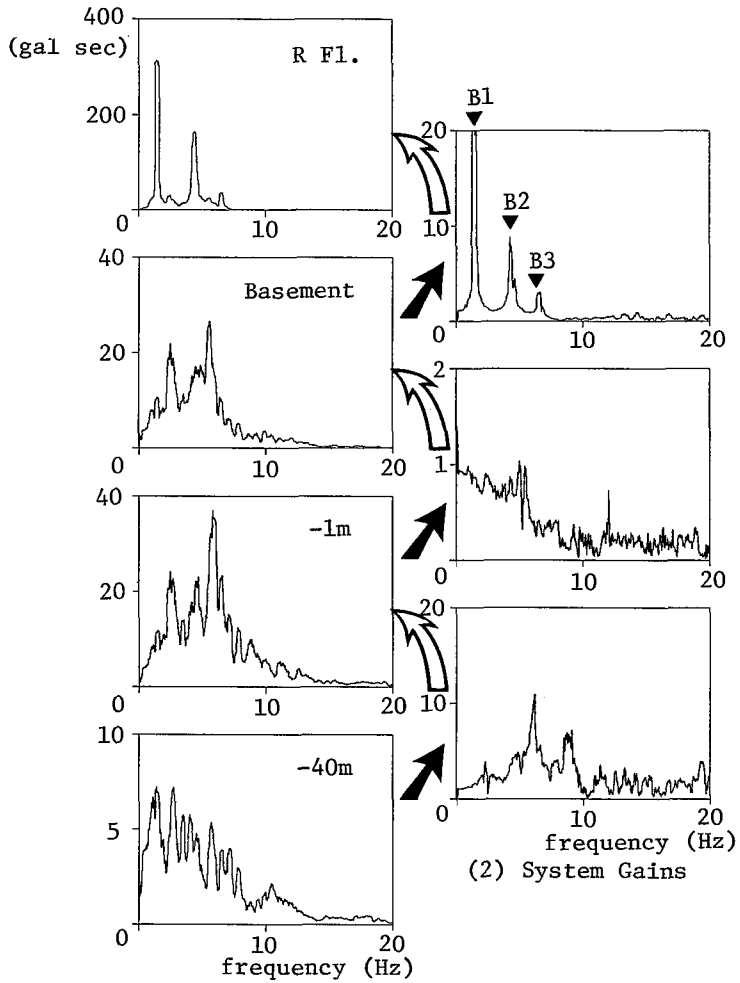

(1) Smoothed Fourier Amplitude Spectra

Fig. 11 FOURIER SPECTRA AND SYSTEM GAINS (MODEL NO.1, Y-DIRECTION)

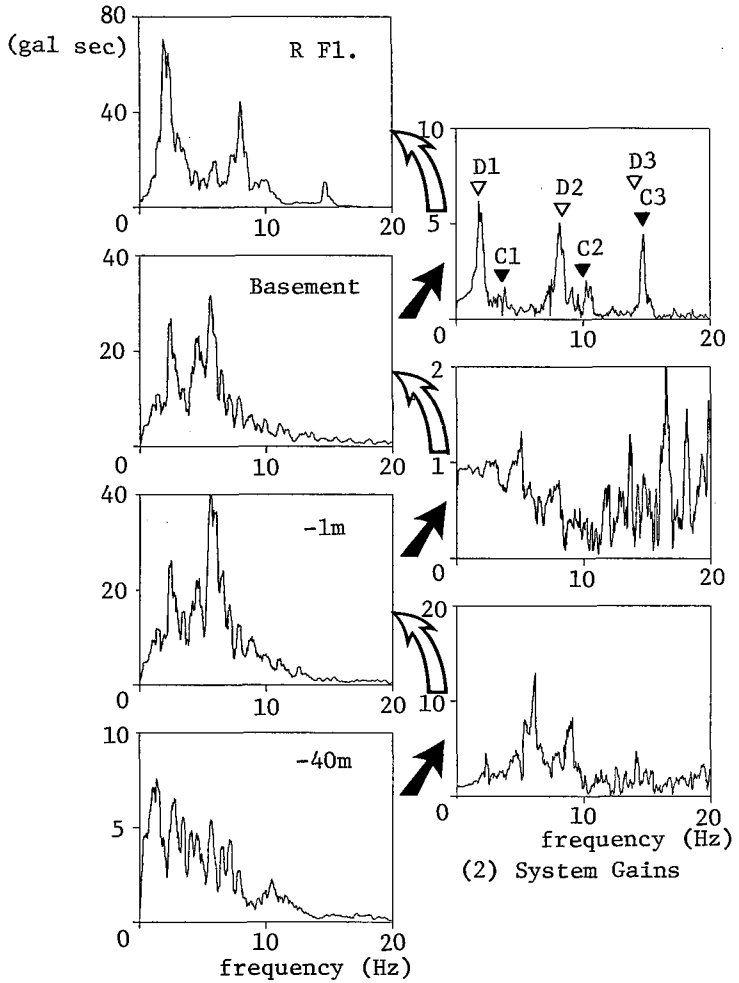

(1) Smoothed Fourier Amplitude Spectra

Fig. 12 FOURIER SPECTRA AND SYSTEM GAINS (MODEL NO.2, X-DIRECTION)

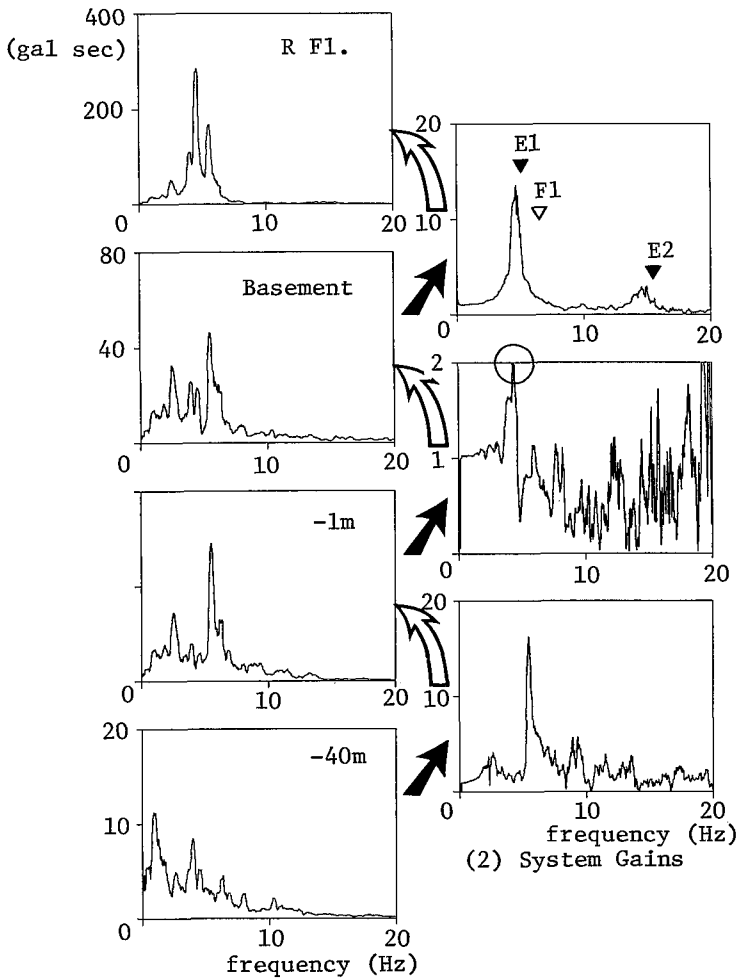

(1) Smoothed Fourier Amplitude Spectra

Fig. 13 FOURIER SPECTRA AND SYSTEM GAINS (MODEL NO.2, Y-DIRECTION)

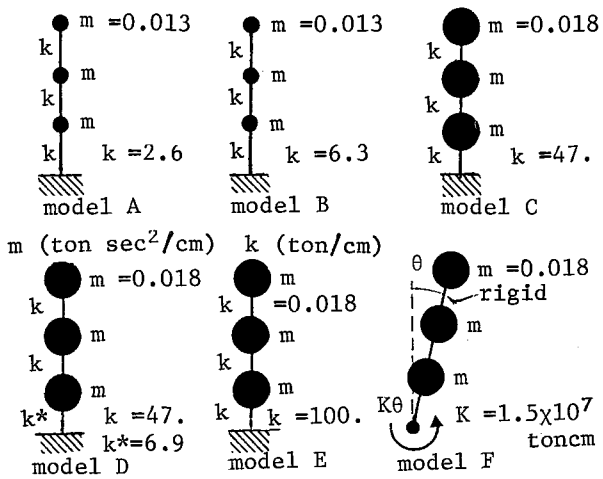

Fig. 14 ANALIZED VIBRATIONAL SYSTEMS

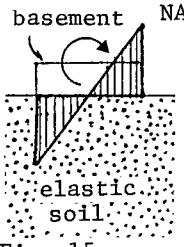

Fig. 15 TRIANGULAR STRESS CONDITIONS

Table 4 CALCULATED NATURAL FREQUENCIES

	1st	2nd	3rd
A	1.0	2.8	4.1
B	1.6	4.4	6.3
C	3.6	10.0	14.6
D	1.7	8.4	14.1
E	5.3	14.8	21
F	7.0	—	—

(Hz)

Table 5 ON-LINE SIMULATION

Excitation	El Centro NS 10 sec + Free Vibration 10 sec		
Peak Excitation	Phase I	130 gal	
	Phase II	160 gal	
Assumed Mass	1.53×10^{-2} tcm^{-1} sec^2 per each floor		
Coefficient used in Consideration of P-Δ effect (t/cm)	1st Story	-0.45	
	2st Story	-0.30	
	3st Story	-0.15	
Test Speed	1/100 of Real Time		
Peak Response Displacement (cm)	Phase I	1st Floor	1.98
		2nd Floor	3.38
		3rd Floor	3.98
	Phase II	1st Floor	6.16
		2nd Floor	7.20
		3rd Floor	7.57

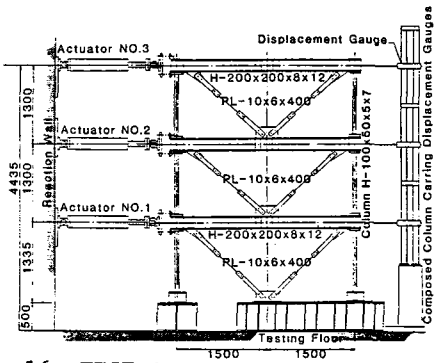

Fig. 16 TEST SETUP FOR PSEUDO-DYNAMIC ON-LINE SIMULATION

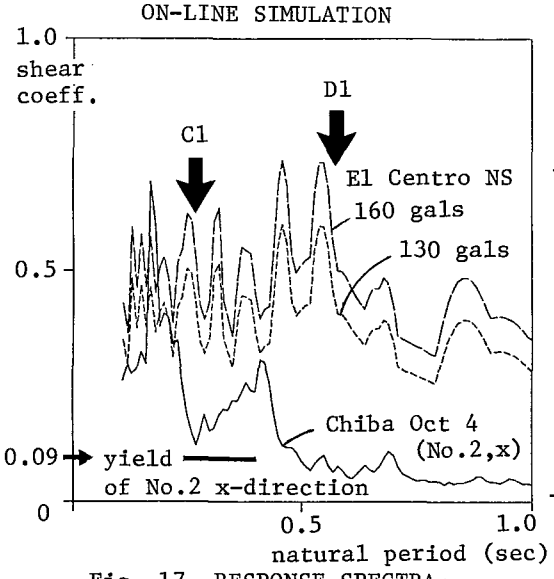

Fig. 17 RESPONSE SPECTRA OF SHEAR COEFFICIENT

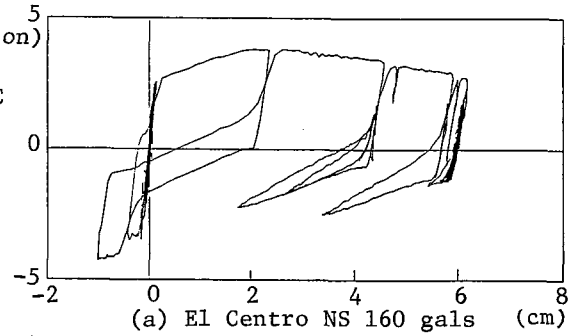

(a) El Centro NS 160 gals

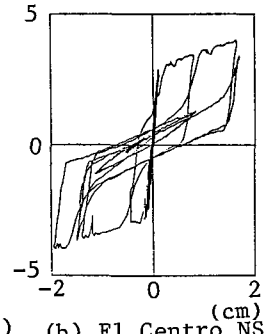

(b) El Centro NS 130 gals

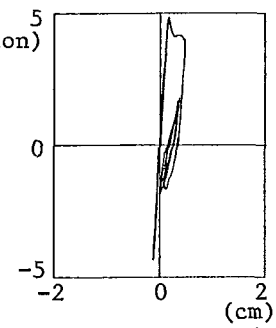

(c) Chiba Oct. 4

Fig.18 COMPARISON OF HYSTERESIS LOOPS